

Phase diagram of Nambu–Jona-Lasinio model with dimensional regularization

T. Inagaki^a, D. Kimura^b, H. Kohyama^c, A. Kvinikhidze^d

^a *Information Media Center, Hiroshima University, Higashi-Hiroshima, Hiroshima 739-8521, Japan*

^b *Faculty of Education, Hiroshima University, Higashi-Hiroshima, Hiroshima 739-8524, Japan*

^c *Department of Physics, Chung-Yuan Christian University, Chung-Li 32023, Taiwan*

^d *A. Razmadze Mathematical Institute, Tbilisi State University,*

Abstract

We investigate the phase diagram on temperature-chemical potential plane in the Nambu–Jona-Lasinio model with the dimensional regularization. While the structure of the resulting diagram shows resemblance to the one in the frequently used cutoff regularization, some results of our study indicate striking difference between these regularizations. The diagram in the dimensional regularization exhibits strong tendency of the first order phase transition.

Keywords: QCD phase diagram, Chiral symmetry, Effective field theory

1. INTRODUCTION

The phase diagram of the quark matter has been actively investigated for decades [1]. Quarks are confined inside hadrons and can not be observed as free particles at low energy. On the other hand at high energy, quarks become free particles due to the asymptotic freedom of the strong interaction. Therefore, it is expected that quarks undergo the phase transition between confined and deconfined states which is one of the most important issues in the theoretical and experimental particle physics.

The fundamental theory to describe quark matter is quantum chromodynamics (QCD), the theory of strong interaction. It is, however, not practical to extract reliable predictions at low energy due to the necessity of complicated nonperturbative calculations in this area. For this reason some effective approaches are used such as the Nambu–Jona-Lasinio (NJL) model [2] and its Polyakov-loop incorporated version, the PNJL model [3], the linear sigma model [4], the chiral perturbation theory [5], the lattice QCD simulations [6].

In this letter, we will consider the NJL model known as a low-energy effective theory of QCD (for reviews, see, [7, 8, 9, 10]). At low temperature, T , and chemical potential, μ , constituent quarks are heavy due to the chiral symmetry spontaneous breaking while they are expected to be light at high T and/or μ where the chiral symmetry is getting restored. Thus the quark system is closely related to the phenomenon of the chiral phase transition. The NJL model actually predicts the chiral symmetry breaking at low energy and its restoration at high energy. Many investigations of the phase diagram are based on the NJL and PNJL models (see, e.g., [11, 12, 13, 14, 15, 16, 17, 18, 19, 20] and [21, 22, 23, 24, 25]).

Since the NJL model is not renormalizable, the model predictions inevitably depend on a regularization procedure applied. The most frequently used method is probably the three-momentum cutoff regularization which introduces the cutoff scale Λ . The model in the cutoff scheme may miss an important contribution when the quark density becomes comparable to the cutoff scale. There is an alternative method, the dimensional regularization (DR), to avoid the issue [26]. In the DR, divergences coming from fermion loop integrals are regularized by lowering the dimension of the integration through an analytic continuation in the dimension variable. Using various regularization ways is interesting, because we believe that the regularization scheme is a dynamical part of the NJL model, it is related to the size and shape of the

effective quark interaction as discussed in [27]. It was found that the model with the DR nicely describes quark systems at low energy, such characteristics as the phase structure and meson properties [26, 27, 28, 29].

We shall study in this article the phase diagram in the three flavor NJL model with the DR. It is interesting because the recent work by the present authors [27] indicates that the phase structure, especially the order of the transition, may differ drastically from the one in the cutoff regularization.

The structure of this letter is following: In Sec. 2, the three flavor NJL model and its parameters are presented. Sec. 3 is devoted to the explanation on the procedure of drawing the phase diagram. We then display the resulting phase diagram of the model in Sec. 4. The concluding remarks are given in Sec. 5.

2. Three flavor NJL model

2.1. The model

The Lagrangian of the three flavor model is

$$\mathcal{L}_{\text{NJL}} = \sum_{i,j} \bar{q}_i (i\cancel{\partial} - \hat{m})_{ij} q_j + \mathcal{L}_4 + \mathcal{L}_6, \quad (1)$$

$$\mathcal{L}_4 = G \sum_{a=0}^8 \left[\left(\sum_{i,j} \bar{q}_i \lambda_a q_j \right)^2 + \left(\sum_{i,j} \bar{q}_i i\gamma_5 \lambda_a q_j \right)^2 \right], \quad (2)$$

$$\mathcal{L}_6 = -K [\det \bar{q}_i (1 - \gamma_5) q_j + \text{h.c.}]. \quad (3)$$

where \hat{m}_{ij} represents the diagonal mass matrix $\text{diag}(m_u, m_d, m_s)$ with flavor indices i, j . G and K are the four- and six-fermion couplings, λ_a are the Gell-Mann matrices in flavor space with $\lambda_0 = \sqrt{2/3} \cdot \mathbf{1}$. The determinant in \mathcal{L}_6 runs over flavor space, so this leads to the six-point interaction known as Kobayashi-Maskawa 't Hooft (KMT) term [30].

The vacuum of the model is determined by the minimum of the thermodynamic potential $\Omega = -\ln Z/(\beta V)$ with the partition function Z , the inverse temperature $\beta = 1/T$, and the volume of the system V . Applying the mean-field approximation, we can calculate the potential Ω in the imaginary time formalism,

$$\Omega = \Omega_v + \Omega_0 + \Omega_T, \quad (4)$$

$$\Omega_v = 2G(\phi_u^2 + \phi_d^2 + \phi_s^2) - 4K\phi_u\phi_d\phi_s, \quad (5)$$

$$\Omega_0 = -\frac{2^{D/2}N_c}{2} \int \frac{d^{D-1}p}{(2\pi)^{D-1}} [E_u + E_d + E_s], \quad (6)$$

$$\Omega_T = -\frac{2^{D/2}N_c}{2} T \int \frac{d^{D-1}p}{(2\pi)^{D-1}} \sum_{i,\pm} \ln [1 + e^{-\beta E_i^\pm}]. \quad (7)$$

Here Ω_v corresponds to the vacuum contribution by the chiral condensates, Ω_0 and Ω_T denote the temperature independent and dependent contributions, $\phi_i (\equiv \langle \bar{i}i \rangle)$ is the chiral condensate for each quark which is the order parameter of the model, $N_c (= 3)$ is the number of colors. D denotes dimensions in the fermion loop integral, $E_i = (p^2 + m_i^{*2})^{1/2}$ is the energy of the quasi-particle with the constituent quark mass m_i^* , $E_i^\pm = E_i \pm \mu$ with a quark chemical potential $\mu (= \mu_u = \mu_d = \mu_s)$.

The fermion loop integral in Eq.(6) diverges, therefore we will perform the analytic continuation in D to regularize it by decreasing the dimension D as discussed in [29, 27]. In the cutoff scheme, the divergent contribution is dropped by introducing the momentum cutoff Λ . To be more precise, the regularization in the DR and cutoff schemes are performed by the following replacements

$$\int \frac{d^{D-1}p}{(2\pi)^{D-1}} \rightarrow \frac{2(4\pi)^{-(D-1)/2}}{\Gamma[(D-1)/2]} M_0^{4-D} \int_0^\infty dp p^{D-2}, \quad (8)$$

$$\int \frac{d^{D-1}p}{(2\pi)^{D-1}} \rightarrow \frac{1}{2\pi^2} \int_0^\Lambda dp p^2, \quad (9)$$

where M_0 is the renormalization scale which is needed to render physical quantities correct mass dimensions. As mentioned in the introduction, the constituent quark mass

$$m_i^* = m_i - 4G\phi_i + 2K\phi_j\phi_k, \quad (i \neq j \neq k) \quad (10)$$

is closely related to the chiral symmetry breaking, namely to the value of ϕ_i . The self-consistent gap equations (10) are obtained as the condition for the thermodynamic potential to be at the extremum, $\partial\Omega/\partial\phi_i = 0$. Eqs (10) explicitly show that the difference between constituent and current quark masses is due to the underlying chiral symmetry breaking.

2.2. Model parameters

The NJL model with the dimensional regularization has 7 free parameters: current quark mass m_u, m_d, m_s , the four- and six-point couplings G, K , the dimension D , and the renormalization scale M_0 .

We consider, for simplicity, the isospin symmetric case, $m_d = m_u$, and set several values for m_u ($= 3, 4, 5, 5.5, 6\text{MeV}$). We then fix the remaining parameters by choosing 5 physical quantities among listed below:

$$\begin{aligned} m_\pi &= 138\text{MeV}, & f_\pi &= 92\text{MeV}, \\ m_K &= 495\text{MeV}, & m_{\eta'} &= 958\text{MeV}, \\ m_\eta &= 548\text{MeV}, & \chi^{1/4} &= 170\text{MeV}. \end{aligned} \quad (11)$$

Following [27], we name the parameter sets as Case χ and m_η depending on which quantities are selected. The Case χ (m_η) is fitted by $\{m_\pi, f_\pi, m_K, m_{\eta'}, \chi(m_\eta)\}$. The parameter setting was performed in [29], and we shall employ three parameter sets, Case m_η^{LD} , m_η and χ , which are shown in Tabs. 1, 2 and 3. Note that

Table 1: Case m_η^{LD} .

m_u	m_s	G	K	M_0	D
3.0	84.9	-0.0195	9.02×10^{-7}	118	2.29

Table 2: Case m_η .

m_u	m_s	G	K	M_0	D
3.0	79.0	-0.0130	2.29×10^{-7}	107	2.37
4.0	106	-0.00748	8.26×10^{-8}	92.0	2.52
5.0	134	-0.00357	1.99×10^{-8}	73.2	2.69
5.5	147	-0.00231	8.40×10^{-9}	62.4	2.77
6.0	162	-0.00142	3.23×10^{-9}	50.9	2.87

Table 3: Case χ .

m_u	m_s	G	K	M_0	D
3.0	77.1	-0.0168	2.23×10^{-7}	120	2.28
4.0	106	-0.0143	2.11×10^{-7}	116	2.36
5.0	134	-0.0119	1.80×10^{-7}	112	2.43
5.5	150	-0.0109	1.62×10^{-7}	110	2.47
6.0	166	-0.00992	1.48×10^{-7}	109	2.50

the Case m_η has two parameter sets for $m_u = 3\text{MeV}$; to distinguish between them we use the superscript LD (lower dimension).

For the sake of comparison we also align the parameters of the cutoff case in Tab. 4. In the cutoff case, we fix 4 parameters, m_s, G, K and Λ with $\{m_\pi, f_\pi, m_K, m_{\eta'}\}$. Unfortunately, there is no solution to simultaneously reproduce the above listed quantities for $m_u \gtrsim 5.87\text{MeV}$.

m_u	m_s	$G\Lambda^2$	$K\Lambda^5$	Λ
3.0	89.5	1.55	8.34	960
4.0	110	1.60	8.38	797
5.0	128	1.71	8.77	682
5.5	136	1.81	9.17	630
5.87	139	2.09	10.1	580

3. Critical behavior

In this section we explain how to draw the phase diagram of the model through the analysis of the thermodynamical potential and the gap equations.

A critical temperature T_c or chemical potential μ_c are given by the maxima of

$$\frac{\partial\phi_u}{\partial t}, \quad (t = T \text{ or } \mu). \quad (12)$$

In fact we apply $t = T$ (μ) for low μ (T) in crossover region. The above quantity becomes infinite at T_c (μ_c) when the transition is of the first order. In this case we determine the transition boundary by the point where the discontinuous change of the chiral condensate ϕ_u occurs by directly searching the minimum of the thermodynamic potential. It is obvious that this procedure is consistent with the criterion of Eq. (12), because a divergent point coincides the maximum point.

3.1. Thermodynamic potential

To see the tendency of the phase transition, we show the behavior of $\Omega(= \Omega(\phi_u, \phi_s) - \Omega(0, 0))$ for the Case m_η and Cutoff with $m_u = 4\text{MeV}$ near the transition boundary in Fig. 1. The curves are plotted along

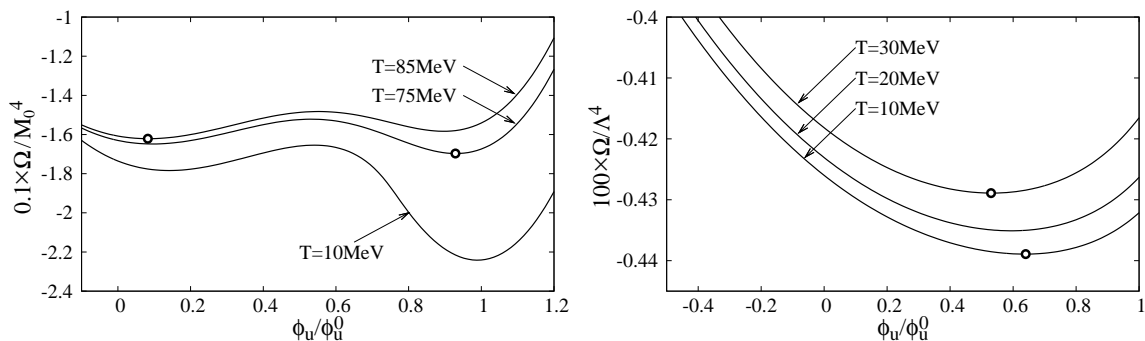


Figure 1: Left panel: $0.1 \cdot \Omega / M_0^4$ along the line $\phi_s = 0.36\phi_u + 0.83\phi_u^0$ in the Case m_η with $m_u = 4\text{MeV}$ for $T = 10, 75, 85\text{MeV}$ and $\mu = 480\text{MeV}$. Right panel: $100 \cdot \Omega / \Lambda^4$ along the line $\phi_s = 0.103\phi_u + 1.43\phi_u^0$ in the Case Cutoff with $m_u = 4\text{MeV}$ for $T = 10, 20, 30\text{MeV}$ and $\mu = 290\text{MeV}$. The circles indicate the global minima.

the line $\phi_s = 0.36\phi_u + 0.83\phi_u^0$ for $T = 10, 75$ and 85MeV with $\mu = 480\text{MeV}$ in the left panel, and along the line $\phi_s = 0.103\phi_u + 1.43\phi_u^0$ for $T = 10, 20, 30\text{MeV}$ with $\mu = 290\text{MeV}$ in the right panel. These lines are chosen so as to show the global minima for lower $T = 75(10)\text{MeV}$ and higher $T = 85(30)\text{MeV}$, which are indicated by the circles, near the transition temperature $T_c \simeq 80(20)\text{MeV}$. ϕ_u^0 denotes the chiral condensate ϕ_u at $T, \mu = 0$ for each case.

The striking difference is observed between these figures. There exists a bump between two stable minima in the DR case, which means that the transition is of the first order between $T = 75$ and 85MeV . On the other hand the cutoff case (right panel) produces rather monotonous curves with no bump, which leads

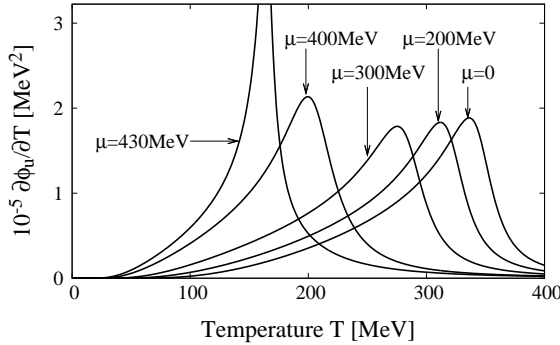


Figure 2: $\partial\phi_u/\partial T$ in the Case m_η with $m_u = 4\text{MeV}$.

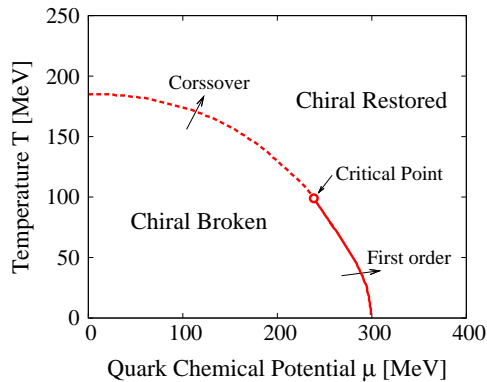


Figure 3: Phase diagram in the Case m_η^{LD} with $m_u = 3\text{MeV}$. The solid (dashed) line represents the first order (crossover) transition. The circle indicates the critical point.

to a smooth crossover. The difference stems from the fact that the ratio of the thermal contribution (μ dependence) $\Omega_T/(\Omega_v + \Omega_0)$ in the DR case is larger than that in the cutoff case at low T . Thus we confirm the stronger tendency of the first order phase transition in the DR scheme.

3.2. $\partial\phi_u/\partial T$

In the crossover region, it is technically easier to analyze Eq. (12) through solving the gap equations because ϕ_u changes continuously with respect to $T(\mu)$. We show the numerical results in Fig. 2. One sees that the maximum point moves toward lower T with increasing μ , and the peak becomes large at high μ . The peak actually diverges when T and μ coincide with the critical point $(T_{\text{CP}}, \mu_{\text{CP}})$. Below T_{CP} , the transition becomes of the first order, and the analysis by Eq. (12) is no longer practically useful for the determination of the transition boundary as mentioned above.

4. Phase diagram

We are now ready to discuss the phase structure of the NJL model with the DR.

4.1. Transition on ϕ_u

Fig. 3 displays the typical structure of the phase diagram in the model with the DR in the Case m_η^{LD} . This is a reasonable picture of a system in the chiral symmetry broken phase at low T and μ , and in the chiral symmetry restored phase at high T and/or μ . The solid (dashed) line represents the first order (crossover)

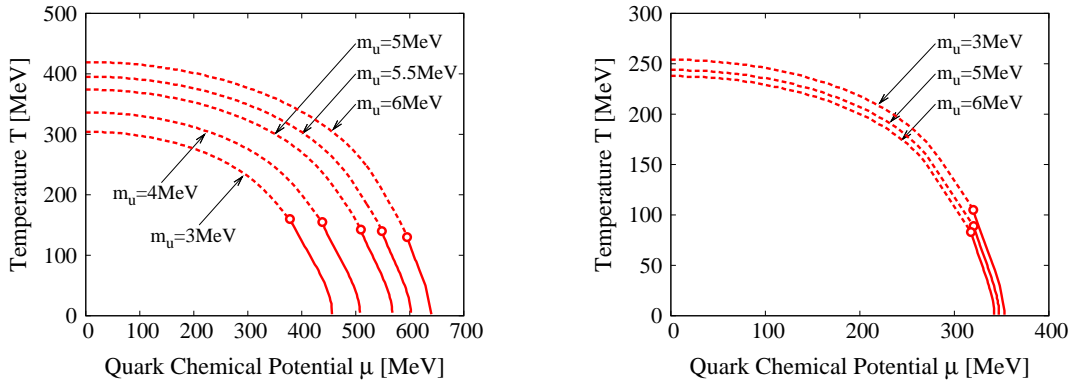


Figure 4: Phase diagrams in the Case m_η and χ are shown in the left and right panels. The solid (dashed) lines represent the first order (crossover) transition. The circles indicate the critical points.

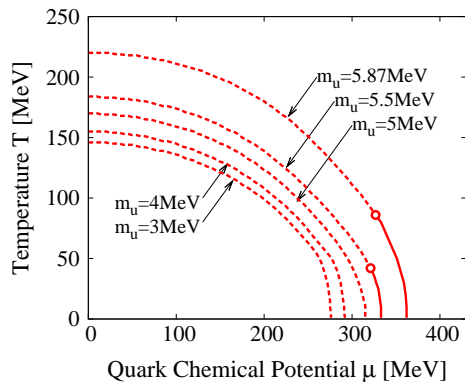


Figure 5: Corresponding diagrams in the Case Cutoff.

transition, and the circle indicates the critical point. Note that the transition temperature, $T_c = 184\text{MeV}$ for $\mu = 0$, is comparable with the lattice QCD prediction, $150 - 200\text{MeV}$. The critical point is located at $(T_{\text{CP}}, \mu_{\text{CP}}) = (99\text{MeV}, 239\text{MeV})$, and it is interesting to see that T_{CP} is close to one obtained in the PNJL model with the cutoff regularization, $T_{\text{CP}} = 102\text{MeV}$, for frequently used parameter set of [9], whereas $T_{\text{CP}} = 48\text{MeV}$ in the NJL model [24]. Note that the obtained critical point is close to one obtained in a NJL type model with the smooth form factor [20], $(T_{\text{CP}}, \mu_{\text{CP}}) = (101\text{MeV}, 211\text{MeV})$, and in the linear sigma model [31], $(T_{\text{CP}}, \mu_{\text{CP}}) = (99\text{MeV}, 207\text{MeV})$. Below we make more detailed comparison between the DR and the cutoff schemes.

Fig. 4 shows the phase diagrams in the Cases m_η and χ for various m_u . We note that in the Case m_η , the region of chiral symmetry broken phase becomes smaller with choosing the smaller value of m_u . On the other hand the Case χ produces similar curves for different m_u . The different behavior can be explained by the fact that the constituent quark mass m_u^* gets smaller with decreasing m_u in the Case m_η , while it almost does not change in the Case χ as discussed in [29]. In the cutoff case (Fig. 5) the region of the chiral symmetry broken state shrinks when m_u is lowered as observed in the Case m_η . It is very interesting to note that the critical point disappears below $m_u = 5\text{MeV}$, where the transition is crossover for all T and μ .

A striking difference between the two regularizations is in that the critical point moves towards higher temperature with decreasing m_u in the DR, while it moves to the opposite direction in the cutoff case. The difference may be understood by observing the value of the six-point coupling K which becomes larger (smaller) with decreasing m_u in the DR (cutoff) procedure, since the KMT term shown in Eq.(3) tends to

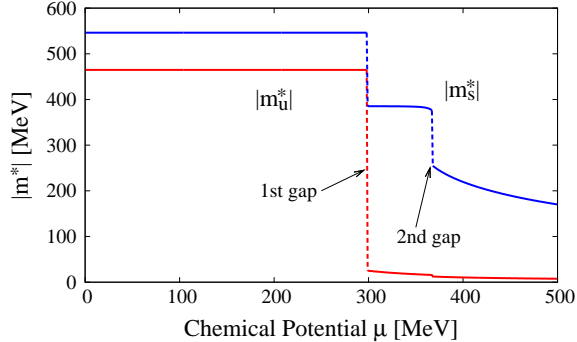


Figure 6: Constituent quark mass $|m_u^*|$ and $|m_s^*|$ for $T = 10\text{MeV}$ in the Case m_η^{LD} with $m_u = 3\text{MeV}$.

drive the first order phase transition [24].

4.2. Partial transition on ϕ_s

As discussed in [27], the constituent quark masses undergo two discontinuous changes at low T in the DR scheme. Fig. 6 displays the typical behavior of $|m_u^*|$ and $|m_s^*|$ as functions of μ at low T ($= 10\text{MeV}$), plotted in the Case m_η^{LD} with $m_u = 3\text{MeV}$. One clearly observes two gaps: one is located around $\mu_c^{(u)} \simeq 300\text{MeV}$ and the other is around $\mu_c^{(s)} \simeq 365\text{MeV}$. Here we call these discontinuities as first and second gaps for lower and higher chemical potential, respectively. The first gap comes from the effect of the approximate $\text{SU}_L(2) \otimes \text{SU}_R(2)$ restoration and the second one comes from that of the partial $\text{SU}_L(3) \otimes \text{SU}_R(3)$ restoration. Thus it may be interesting to study the phase structure concerning the second transition as well.

To draw the phase diagram on the second transition, we set the criterion of the transition by using the following quantity

$$\frac{\partial \phi_s}{\partial t}, \quad (t = T \text{ or } \mu). \quad (13)$$

Then below μ_{CP} , namely in the crossover region, the above quantity has only one maximum, which determines the crossover transition on ϕ_s . While above μ_{CP} the quantity $\partial \phi_s / \partial \mu$ shows non-trivial behavior; it becomes infinite at $\mu_c^{(u)}$, and has second maximum at $\mu_c^{(s)}$. So $\partial \phi_s / \partial \mu$ has typical two maxima at $\mu_c^{(u)}$ and $\mu_c^{(s)}$ below T_{CP} as seen in Fig. 6. Here we call the transition point corresponding to the second maximum, $\mu_c^{(s)}$, “the second phase boundary”. To distinguish between the two phase transitions, we call the transition line on ϕ_u discussed in the previous subsection “the first phase boundary”.

In the phase diagram on the 1st and 2nd phase boundaries (Fig. 7) the dashed and dotted lines represent the crossover transition on ϕ_u and ϕ_s , respectively. The solid line for lower (higher) chemical potential indicates the discontinuous change on the first (second) gap. We see that the crossover line on ϕ_s is observed at a bit lower temperature than that on ϕ_u for $\mu < \mu_{\text{CP}}$. It should be noticed that the critical curves on ϕ_u and ϕ_s intersect at the critical end point $(T_{\text{CP}}, \mu_{\text{CP}})$ on ϕ_u . Because the value of ϕ_s is affected by ϕ_u , as is clearly seen from Fig. 6, ϕ_s shows discontinuous change at the point where ϕ_u has a gap. Then $\partial \phi_s / \partial t$ blows up and approaches to infinity near the critical point where $\partial \phi_u / \partial t$ is divergent. Below T_{CP} , $\partial \phi_s / \partial \mu$ has two maxima appearing at the first gap and higher chemical potential. The first maximum coincides with the red solid line and the second one is plotted by the blue line in Fig. 7. The transition on the second gap also has the critical point whose location is exhibited by the blue circle at higher chemical potential.

We also studied the other Cases, m_η and χ , with various m_u , and found that the qualitative behavior does not show remarkable difference; the critical point on ϕ_s moves toward higher temperature with decreasing m_u as seen in the ϕ_u case. Therefore, we only displayed the Case m_η^{LD} here.

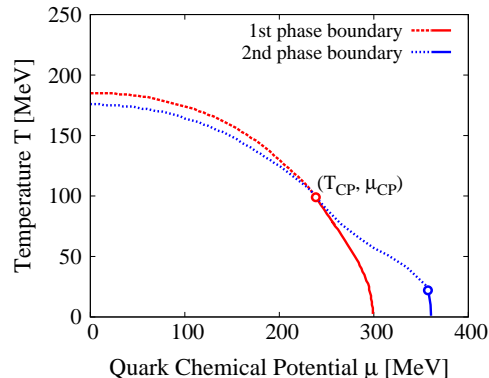


Figure 7: The 1st and 2nd phase boundaries in the Case m_{η}^{LD} with $m_u = 3\text{MeV}$. The red dashed and blue dotted lines represent the crossover transition on ϕ_u and ϕ_s . The red and blue solid lines indicate the transition on the first and second gap, respectively. The circles exhibit the critical points.

5. Concluding remarks

We studied the phase diagram of the NJL model with the DR and cutoff regularization. We found that the phase diagram on the $T - \mu$ plane in the NJL model with the DR shows a stronger tendency of the first order phase transition. The tendency is confirmed by the shapes of the thermodynamic potential shown in Fig. 1 where we find a bump in the DR, and rather monotonous behaviour in the cutoff case.

We have also studied the phase structure on the change of ϕ_s in Sec. 4.2., where we found that the approximate $\text{SU}_L(2) \otimes \text{SU}_R(2)$ symmetry and the partial $\text{SU}_L(3) \otimes \text{SU}_R(3)$ symmetry restore at a similar temperature for low chemical potential, $\mu < \mu_{\text{CP}}$. It may be difficult to distinguish between the two lines experimentally, because the transitions are smooth crossover at low chemical potential.

From the obtained phase diagrams, we conclude that the first order phase transition persists for low m_u in the model with the DR method. The finding is consistent with the current symmetry analysis based consensus [32] stating that the chiral phase transition is of the first order in the chiral limit, $m_{u,d,s} \rightarrow 0$. This tendency may be understood by the following reasoning. The loop contribution from the lower integration momenta is enhanced by lowering dimension. It introduces non-locality in the model with the DR. The infrared behavior of the loop integral is important for thermal corrections. It can rise the critical end point temperature, T_{CP} .

Finally, because the parameter difference crucially affects the location of the critical point as confirmed in this article, we think it is interesting to study the related issues, such as the case with the chiral limit, and the m_u, m_s dependence on the order of the chiral transition in the context of the Columbia plot [33].

Acknowledgments

HK is supported by the grant NSC-99-2811-M-033-017 from National Science Council (NSC) of Taiwan.

References

- [1] For recent reviews, M. A. Stephanov, Prog. Theor. Phys. Suppl. **153** (2004) 139, Int. J. Mod. Phys. A **20** (2005) 4387, PoS LAT **2006** (2006) 024, O. Philipsen, Prog. Theor. Phys. Suppl. **174** (2008) 206, arXiv:1111.5370 [hep-ph], W. Weise, Prog. Theor. Phys. Suppl. **186** (2010) 390, arXiv:1201.0950 [nucl-th], K. Fukushima and T. Hatsuda, Rept. Prog. Phys. **74** (2011) 014001, G. Endrodi, Z. Fodor, S. D. Katz and K. K. Szabo, JHEP **1104** (2011) 001.
- [2] Y. Nambu and G. Jona-Lasinio, Phys. Rev. **122** (1961) 345, **124** (1961) 246.
- [3] K. Fukushima, Phys. Lett. B **591** (2004) 277.
- [4] M. Gell-Mann and M. Levy, Nuovo Cimento **16** (1960) 705.
- [5] J. Gasser and H. Leutwyler, Nucl. Phys. B **250** (1985) 465.
- [6] K. G. Wilson, Phys. Rev. D **10** (1974) 2445.

- [7] U. Vogl and W. Weise, Prog. Part. Nucl. Phys. **27** (1991) 195.
- [8] S. P. Klevansky, Rev. Mod. Phys. **64** (1992) 649.
- [9] T. Hatsuda and T. Kunihiro, Phys. Rept. **247** (1994) 221.
- [10] M. Buballa, Phys. Rept. **407** (2005) 205.
- [11] U. Wolff, Phys. Lett. B **157** (1985) 303.
- [12] T. Hatsuda and T. Kunihiro, Phys. Rev. Lett. **55** (1985) 158.
- [13] F. Karsch, J. B. Kogut and H. W. Wyld, Nucl. Phys. B **280** (1987) 289.
- [14] K. G. Klimenko, Z. Phys. C **37** (1988) 457.
- [15] M. Asakawa and K. Yazaki, Nucl. Phys. A **504** (1989) 668.
- [16] B. Rosenstein, B. Warr and S. H. Park, Phys. Rept. **205** (1991) 59.
- [17] S. Hands, A. Kocic and J. B. Kogut, Nucl. Phys. B **390** (1993) 355.
- [18] P. Zhuang, J. Hufner and S. P. Klevansky, Nucl. Phys. A **576** (1994) 525.
- [19] T. Inagaki, T. Kouno, and T. Muta, Int. J. Mod. Phys. A **10** (1995) 2241.
- [20] J. Berges and K. Rajagopal, Nucl. Phys. B **538** (1999) 215.
- [21] K. Fukushima, Phys. Rev. D **68** (2003) 045004.
- [22] C. Ratti, M. A. Thaler and W. Weise, Phys. Rev. D **73** (2006) 014019.
- [23] S. Roessner, C. Ratti and W. Weise, Phys. Rev. D **75** (2007) 034007.
- [24] K. Fukushima, Phys. Rev. D **77** (2008) 114028, Erratum-ibid. D **78** (2008) 039902.
- [25] T. Hell, S. Roessner, M. Cristoforetti and W. Weise, Phys. Rev. D **79** (2009) 014022, Phys. Rev. D **81** (2010) 074034.
- [26] T. Fujihara, D. Kimura, T. Inagaki, and A. Kvinikhidze Phys. Rev. D **79** (2009) 096008.
- [27] T. Inagaki, D. Kimura, H. Kohyama and A. Kvinikhidze, arXiv:1110.5898 [hep-ph].
- [28] T. Inagaki, D. Kimura, and A. Kvinikhidze, Phys. Rev. D **77** (2008) 116004.
- [29] T. Inagaki, D. Kimura, H. Kohyama, and A. Kvinikhidze, Phys. Rev. D **83** (2011) 034005.
- [30] M. Kobayashi and T. Maskawa, Prog. Theor. Phys. **44** (1970) 1422, M. Kobayashi, H. Kondo, and T. Maskawa, Prog. Theor. Phys. **45** (1971) 1955, G. 't Hooft, Phys. Rev. D **14** (1976) 3432, **18** (1978) 2199(E), Phys. Rept. **142** (1986) 357.
- [31] O. Scavenius, A. Mocsy, I. N. Mishustin and D. H. Rischke, Phys. Rev. C **64** (2001) 045202.
- [32] R. D. Pisarski and F. Wilczek, Phys. Rev. D **29** (1984) 338.
- [33] F. R. Brown *et al.*, Phys. Rev. Lett. **65** (1990) 2491.